J Mater Sci (2011) 46:3291–3308
DOI 10.1007/s10853-010-5216-7

EBSD investigation of the microstructure and microtexture evolution of 1050 aluminum cross deformed from ECAP to plane strain compression

Ehab A. El-Danaf · Mahmoud S. Soliman · Abdulhakim A. Almajd

Received: 13 July 2010 / Accepted: 22 December 2010 / Published online: 8 January 2011

Abstract Electron backscattered diffraction (EBSD) was used to document the microstructure and texture developed due to cross deformation of commercial purity 1050 aluminum alloy. The materials are first deformed in equal channel angular pressing die (ECAP) to different number of passes; 1,4, 8, 12, and 16 passes, via route B_C and then deformed in plane strain compression (PSC) to two axial true plastic strain values of 0.5 and 1.0. Deformation path change was proven to be a very effective tool for manipulating the evolution of microstructure and microtexture. The study provides a documentation of the evolution of microstructure parameters namely cell size, misorientation angle, fraction of submicron grain size, and fraction of high angle grain boundaries. These microstructure parameters were investigated on two planes; the plane normal to the loading direction in PSC (RD–TD) and that plane normal to the transverse direction (RD–ND). These microstructure parameters are compared to those achieved due to the ECAP process only. The ideal rolling texture orientations are depicted and crystal orientation maps were generated. The spatial distribution of grains having these orientations is revealed through these maps. The fraction of the main texture components for a 10° spread around the specified orientations is experimentally calculated and a quantitative idea on the evolution of microtexture is also presented.

E. A. El-Danaf · M. S. Soliman · A. A. Almajd
Mechanical Engineering Department, College of Engineering, King Saud University, P.O. Box 800, Riyadh 11421, Saudi Arabia

E. A. El-Danaf (✉) · M. S. Soliman · A. A. Almajd
Center of Excellence for Research in Engineering Materials (CEREM), College of Engineering, King Saud University, Riyadh, Saudi Arabia
e-mail: edanaf@ksu.edu.sa

Introduction

Equal channel angular pressing die (ECAP) is a promising process for the production of ultrafine-grained (UFG) structure in bulk materials. There has been a great interest over the last two decades [1–3] in the development of UFG structures through studying different ECAP parameters (die channel angle, number of pressings, processing route or in other words billet rotation between passes, relief angles in the die, back pressure, friction, pressing speeds, and ECAP processing temperature). When the sample is pressed through several consecutive passes, the shearing characteristics may be changed by rotating the sample between each pass. Thus, the route with which the sample was re-entered to the ECAP die in each pass has an influence on the microstructure and texture achieved [4, 5] due to successive change of the shear plane. ECAP was found to be an effective technique to control texture strength and crystallographic orientation. Compared to conventional techniques, ECAP offers a large variety of parameters for controlling textures, of which the most obvious are the number of passes, the processing route, due to the frequent strain path changes and severe plastic deformation involved and presence of back pressure. Initial texture was seen [6] to play a limited role on texture orientations and a significant role on texture strength at the earliest stage of deformation. Zhilyaev et al. [7] demonstrated that with back pressure, texture corresponded more closely with the idealized model of ECAP involving shear on the plane of the die channel intersection.

Iwahashi et al. [4] have investigated the process of grain refinement and development of subgrain misorientation, using transmission electron microscopy and selected area electron diffraction, on 99.99 pct aluminum processed from 1 to 4 passes in ECAP using different processing routes.

They ascertained that with a single pressing, there is a development of subgrain bands with small misorientations. They also found that microstructure development depended on the processing route, and found that the subgrain evolved more rapidly into arrays of high angle boundaries using route B_C in which the sample was rotated by 90° between each pressing. Gholinia et al. [8] have used scanning electron microscope equipped with electron backscattered diffraction (EBSD) analysis system and provided different conclusions in regard to the superiority of a certain route in which the subgrains evolve most rapidly to high angle grain boundaries. Sun et al. [5] have attributed these contradictions to the use of different composition materials, different characterization methods and different characterization parameters that are used to identify the processed microstructure. Processing route is also reported to affect the texture developed, previous work by Salem et al. [9] reported that the texture strength developed in route C is higher compared to route B_C in commercially pure aluminum, up to four passes. Another recent work[10] done on aluminum to eight passes via route C and B_C, also demonstrated the fact that the strength of the texture develop differently, as the results ascertained that the texture strength in route C is much higher than that developed in route B_C. Also, the study showed that the difference can be in the distribution of texture intensity around the three main identified texture fibers.

Lapovok et al. [11] investigated ECAP of AA 6111 sheets used in automotive industry. It was determined that ECAP is able to refine the grain size of the sheet, diminish the detrimental as-rolled texture components in the sheet and retain an acceptable level of bi-axial ductility such as is required during the automotive forming process. It was reported that route A, after two passes, produced marginally improved properties with respect to texture and formability compared to the same sheet exposed to only a single pass.

Li et al. [12] have measured the texture developed in one pass in aluminum and demonstrated that these ECAP texture orientations can be derived from those for negative simple shear, by increasing the ϕ_1 of simple shear ideal orientations by 45°, which is the angle that transforms the shear reference system $X'Y'Z'$ to the billet axes system XYZ in a 90° channel ECAP die, while the other two Euler angles remain the same (please refer to Fig. 1, where an ECAP processed billet is displayed and the two sets of axes are shown). These orientations distribute along two partial fibers, similar to the development of $\{111\}\ \langle uvw\rangle$ and $\{hkl\}\ \langle 110\rangle$ partial fibers in simple shear deformation of fcc materials. The two partial fibers that constitutes the texture orientations after 1 ECAP pass are designated $\{111\}_\theta\ \langle uvw\rangle$ with a $\{111\}$-plane counter clockwise rotated (CCW) by 45° about the Z-axis towards the Y'-axis

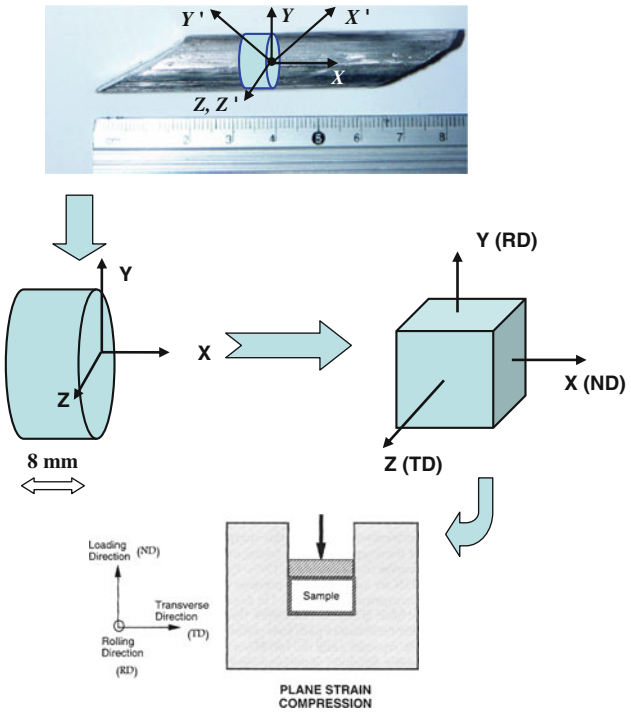

Fig. 1 A schematic that shows the sequence of conducting the experiments

and the other designated as $\{hkl\}\ \langle 110\rangle_\theta$ with a $\langle 110\rangle$ direction CCW rotated by 45° about the Z-axis towards the X'-axis.

Plane strain compression (PSC) simulates the rolling operation, as it imposes the same state of strain. The constrained direction in the die, used to apply a state of plane strain, resembles the transverse direction in rolling (please see Fig. 1, where other directions are also indicated). Shear banding (strain localization in deformation bands) is a dominant deformation mode in rolling, and thus consequently in PSC, at moderate and large deformation levels. Shear bands consist of very small elongated crystallites that are separated by high angle boundaries. Duggan et al. [13], using the STEM technique, have reported that these crystallites exhibits distinct preference towards the Goss orientation $\{1\ 1\ 0\}\ \langle 0\ 0\ 1\rangle$. Shear bands occurs on different scales [14]: grain-scale shear bands (microscopic), which extend through one or a few grains; and sample-scale shear bands (macroscopic), which extend through the entire sample. Therefore, there is a tendency to regard shear bands as a failure mode, as they provide an easy crack propagation path. It has been reported [13] that in rolling these bands form as thin planar sheets that are parallel to the transverse direction and inclined about 25°–40° to the rolling direction.

The propensity of shear banding in PSC is well established [14, 15]. It is believed that the limited choices of

shearing planes in PSC enhances greatly the chance of cooperation of slip in neighboring grains by promoting appropriate lattice rotations that will align the most active slip planes in these grains thus leading to macroscale shear bands. Leffers and Sorenson [16] proposed that the rotation of the {111} planes to approximately being parallel to the rolling plane makes homogeneous slip on these planes extremely difficult and this leads to inhomogeneous deformation through shear bands. Sevillano et al. [17] have argued that shear bands can occur only if a critical cold-worked state is established and that the formation of shear bands is energetically favored over homogenous deformation in anisotropic material. A recent work [15] on a group of high, medium, and low stacking fault energy fcc metals and alloys has ascertained that shear banding is promoted by small grain size.

The texture development of cold rolled fcc metals can best be described by orientation concentrations along two fibers, the α fiber ($\langle 110 \rangle$ parallel to the sheet normal) and the β fiber ($\langle 110 \rangle$ tilted 60° towards the rolling direction). These are usually called skeleton lines, which are mainly determined by connecting the density maxima in the different orientation distribution function sections. The density along these lines has been repeatedly discussed in literature [18, 19]. The α fiber extends from the Goss (G) orientation $\{0\ 1\ 1\}\ \langle 1\ 0\ 0 \rangle$ to the $\{0\ 1\ 1\}\ \langle 2\ 1\ \bar{1} \rangle$ B orientation (brass component). The β fiber extends through three main components $\{1\ 1\ 2\}\ \langle 2\ 1\ \bar{1} \rangle$, $\{1\ 2\ 3\}\ \langle 6\ 3\ \bar{4} \rangle$, $\{0\ 1\ 1\}\ \langle 2\ 1\ \bar{1} \rangle$ which are referred to as Cu (copper), S, and B (brass) orientations, respectively. The texture of different fcc alloys differ mainly in the volume fractions of these components. It has been always reported that rolling of medium and high stacking fault energy metals yields copper type texture, and rolling of low stacking fault energy metals develops a brass type texture.

Combining ECAP with subsequent another deformation mode offers additional opportunity for texture control. Ferrase et al. [20] have combined ECAP with rolling and stated that with ECAP using route A and B_C there is a global decrease of texture strength in accordance with other work [21, 22] and attributed this to mechanically induced dynamic recrystallization, which occurs at high level of deformation and promoted grain rotation and grain boundary sliding. They have noted that moderate rolling reductions (50–75%) were sufficient to create rolling textures, and that beyond reductions of 95% texture softening due to orientation spreading was observed.

The objective of the current work is to document the development of microstructure and texture of plane stain compressed samples that were previously subjected to different number of ECAP passes, up to 16 passes, via route B_C.

Experimental procedure

The ECAP die is designed and manufactured from three assembled tool steel blocks. The die angles were taken to be: $\Psi = 0$ and $\phi = 90°$. Route B_C, where the sample was rotated by 90° between subsequent pressings, is adopted. Commercial purity aluminum (1050) with purity of 99.5% was used in this study. The material was supplied as cold rolled plates of 15 mm thickness. Cylindrical samples of 12 mm diameter were machined parallel to the rolling direction, and then annealed at a temperature of 600 °C for 8 h, giving a grain size of about 600 μm. The annealed samples were lubricated using graphite-based lubricant and pressed in the ECAP die at speed of 10 mm/min using an Instron machine. The samples were processed to 1, 4, 8, 12, and 16 passes.

Discs of about 8 mm in thickness were cut from the ECAP processed samples as seen in Fig. 1, and then further machined to produce almost cubic samples of sides of about 8 mm. These cubic samples were inserted into another die that applied a state of plane strain condition, during loading (see Fig. 1). The surfaces were carefully marked to maintain the *X*-plane as the loading surface, the *Y*-plane as the rolling direction, and the *Z*-plane as the transverse direction in the PSC die. Two samples of each ECAP processed material were plane strain compressed to two strain levels of 0.5 and 1.0, respectively. These strains are the true axial stains in the loading direction (ND). PSC tests were performed using an Instron machine with a constant speed of 0.5 mm/min. Teflon sheet and high pressure grease were used to nearly isolate the effect of friction.

Samples after PSC were investigated on two planes; one is RD–TD and the other is the RD–ND. Samples were electropolished on these two planes, and the grain structures and texture were recorded by orientation imaging microscopy (OIM) using the EBSD technique integrated in Jeol SEM (controlled and analyzed using TSL software). EBSD has the advantage of rapidly gathering large amounts of quantitative data over larger areas while maintaining the ability to characterize cell and subgrain boundaries. The EBSD scanning parameters were set such that a grain boundary was defined when the misorientation between two adjacent measurement points was greater than 2°, thus it should be emphasized that grain boundaries with misorientation below 2° are not seen. In the work by Mishra et al. [23], they have used TEM in combination with EBSD equipped with TSL set up to ensure precision and determine the correct scanning parameters. They came to the conclusion that the step size has to be reduced from 0.5 to 0.2 μm in the samples subjected to two or more ECAP passes to capture the correct microstructural features. They have also reduced the scan area to 50 μm × 50 μm to be able to complete the experiments in a reasonable

Table 1 Main ideal orientations of rolling texture in fcc metals considered in the this study

Notation	Miller index $\{hkl\}\ \langle uvw\rangle$	Euler angles (°)		
		ϕ_1	ϕ	ϕ_2
Cu	$\{1\ 1\ 2\}\ \langle 1\ 1\ \bar{1}\rangle$	90	35	45
B	$\{0\ 1\ 1\}\ \langle 2\ 1\ \bar{1}\rangle$	35	45	0
S	$\{1\ 2\ 3\}\ \langle 6\ 3\ \bar{4}\rangle$	59	37	63
G	$\{0\ 1\ 1\}\ \langle 1\ 0\ 0\rangle$	0	45	0

time. They also implemented a grain tolerance angle of 5° and ascertained that the grain size as predicted from EBSD data was shown to be larger than the actual value measured in TEM. This is the reason behind the 2° tolerance angle selected in the present work. Also, in the present work the step size was taken in the range of 0.05–0.1 μm in all scans performed as this is expected to be less than the grain size anticipated as well as lower than the recommended value by Mishra et al. [23]. The scan areas were taken 50 μm × 50 μm for almost all samples.

The main theoretical ideal orientations that reflect the rolling textures in fcc metals considered in this study can be seen in Table 1. However, because of the cubic crystal symmetry of aluminum alloys, and because of the specimen symmetry at rolling, orthotropic symmetry, it is possible to reduce the angular range to $0° \leq \phi_1 \leq 90°$; $0° \leq \phi \leq 90°$; $0° \leq \phi_2 \leq 90°$ in which each orientation occurs at least once. A terminology that will be used here in coding the samples is as follows: "E" for ECAP processed samples and then plane strain compressed. The number that comes after "E" is the number of ECAP passes as a pre-state for the PSC. The number that comes after that refers to the amount of axial true strain imposed in plane strain (E105, corresponds to a sample ECAPed to 1 pass and then plane strain compressed to 0.5; E11, corresponds to a sample ECAPed to 1 pass and then plane strain compressed to 1.0; E1605, corresponds to a sample ECAPed to 16 passes and then plane strain compressed to 0.5; E161, corresponds to a sample ECAPed to 16 passes and then plane strain compressed to 1.0).

Results

Microstructure of cross deformed 1050 aluminum

Microstructure of the ECAP processed samples and subsequently plane strain compressed to an axial true strain of 0.5 and 1.0 is studied on two planes: RD–TD plane (normal to the loading direction) and RD–ND plane (normal to the transverse direction). A sample of this study is presented in Fig. 2a and b for samples E1205, E121, respectively, for the RD–TD plane. Figure 2 represents color-coded maps according to cell size along with the distribution of cell size with grain tolerance angle (GTA) of 2° and a histogram for the statistical variation of angle of misorientation measured from 2° to 65°. The average cell size and the average misorientation angle are annotated on the respective figure sections.

The pattern indexing in OIM is generally quite effective in identifying the orientation from a diffraction pattern. However, sometimes OIM has difficulty identifying some orientations such as at grain boundaries where the patterns are often made up of two superposed diffraction patterns from both crystal lattices separated by the grain boundary. This might lead to erroneous results near boundaries and triple points. Thus, TSL software provided several cleanup methods that generally cleanup individual data points based on the neighboring orientations. Since these methods change the data, utmost care must be taken to avoid introducing artificial trends in the data. The cleanup procedures work best when the grain size anticipated is considerably greater than the step size implemented in the scan. A neighbor orientation correlation cleanup (level 4), followed by a grain confidence index (CI) standardization cleanup with grain tolerance angle of 2° was used for all samples, then a CI filter of 0.05 was implemented to eliminate the points that were not indexed correctly. The first cleaning procedure operates by examining each data point individually to determine if the orientation is different from its immediate neighbors and level 4 is selected as all lower cleanup levels will be performed sequentially. The second cleaning procedure involves changing the confidence index of all points in a grain to the maximum CI found among all points belonging to the grain.

Microtexture of cross deformed 1050 aluminum

Figure 3 represents the (100), (110), and (111) pole figures on the RD–TD plane for the samples that were ECAP processed to different number of passes and further plane strain compressed to a true axial strain of 0.5. Figure 4 presents the pole figures for samples that were ECAP processed and then plane strain compressed to a true axial strain of 1.0. It is noticed from the pole figures that the texture exhibits a clear transition to capture the features of the rolling texture even though the starting texture is totally different in each case. It is reported that texture evolves differently with the number of ECAP passes [24], due to the successive change of the shearing plane associated with rotating the sample between subsequent pressings. A clear view of how the texture in ECAP is distributed among the texture fibers with number of ECAP pressings can be taken from a recent work [24] based also on EBSD that was done on the same batch of material subjected to the same

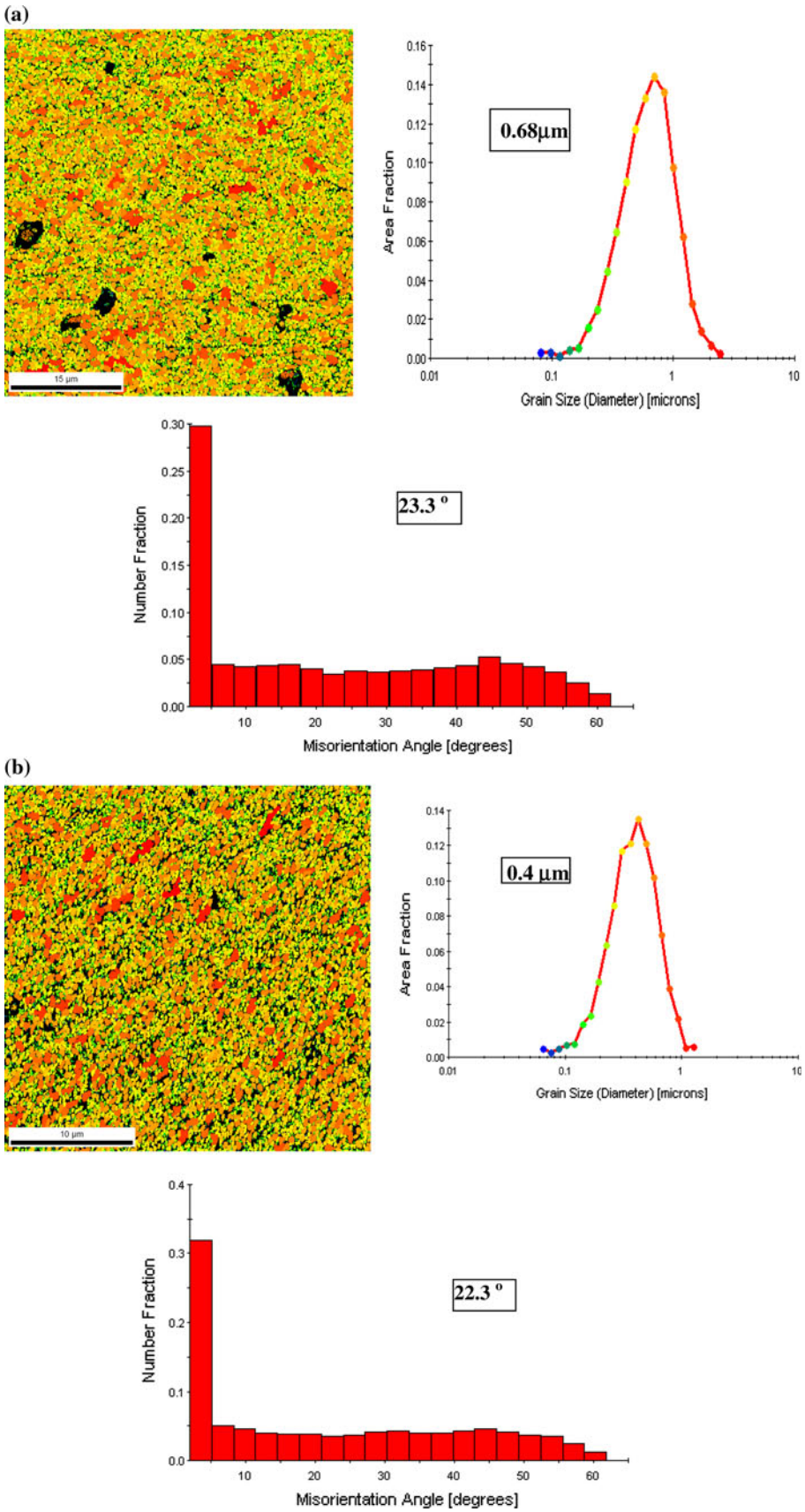

Fig. 2 Color-coded orientation maps, distribution of cell size, and misorientation angle for sample E1205 (**a**) and sample E121 (**b**) for the RD–TD plane

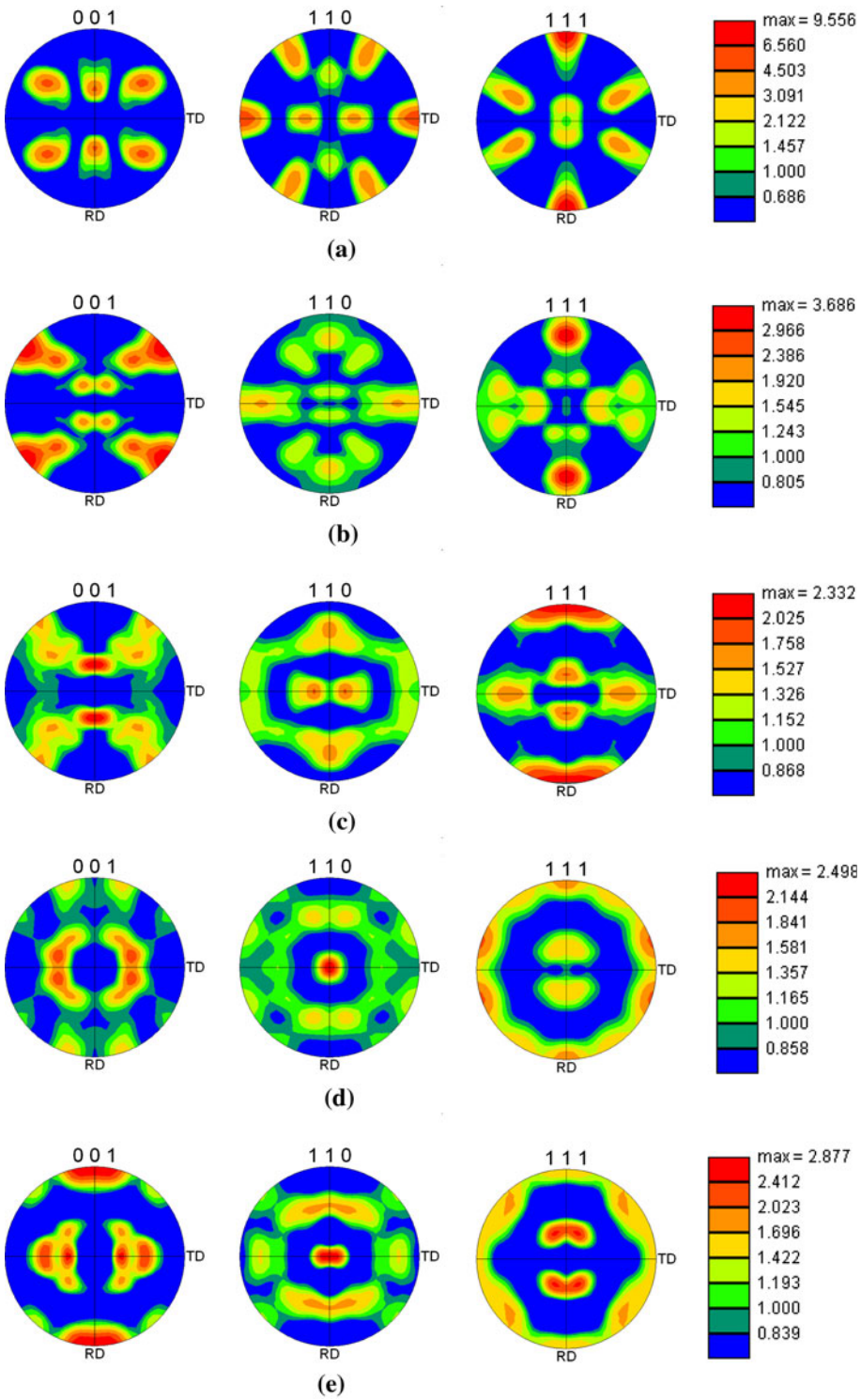

Fig. 3 (100), (110), and (111) pole figures for samples ECAP processed to different number of passes and further plane strain compressed to an axial true strain of 0.5. The number of ECAP passes is 1 (**a**), 4 (**b**), 8 (**c**), 12 (**d**), and 16 (**e**)

annealing treatment. Figure 5a and b represents the pole figures for the sample that is ECAP processed to one pass on the flow plane (X–Y plane, see Fig. 1), and sample E11 on the same plane (RD–ND plane), respectively. It is clear that the texture in (a) exhibits an ideal shear texture and the one in (b) is a rotation by about 45° about ND. Worth to mention is that the grains on the X–Y plane after one ECAP pass were found to be inclined by about 40°–45° to the ECAP extrusion direction (X-axis) and after PSC the grains rotated and became aligned with the rolling direction. This observation is consistent with the 45° rotation in the pole figures. Figure 6a–d presents the orientation distribution function plots (ODF) with constant ϕ_2 sections for samples E1205, E121, E1605, and E161, respectively.

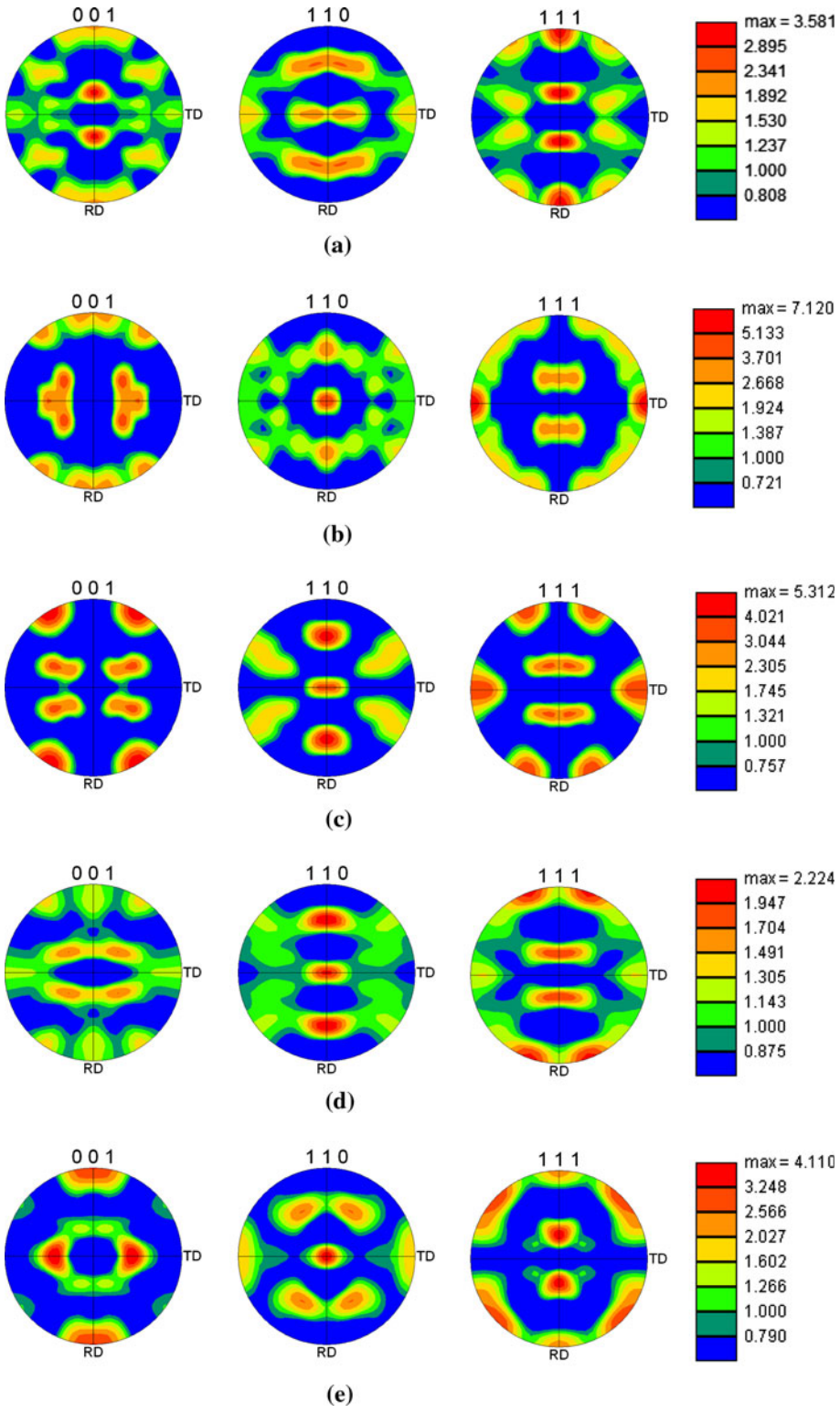

Fig. 4 (100), (110), and (111) pole figures for samples ECAP processed to different number of passes and further plane strain compressed to an axial true strain of 1.0. The number of ECAP passes is 1 (**a**), 4 (**b**), 8 (**c**), 12 (**d**), and 16 (**e**)

Discussions

Evolution of microstructure parameters

Figure 7 represents the results from scanning the RD–TD plane for samples ECAP processed to different number of passes and further plane strain compressed to true axial strains of 0.5 and 1.0. Figure 7a shows the evolution of cell structure size with number of passes. Figure 7b gives the variation of average misorientation angle with number of passes. Figure 7c gives the area fraction of grains less than 1 μm based on a 2° grain tolerance angle. Figure 7d

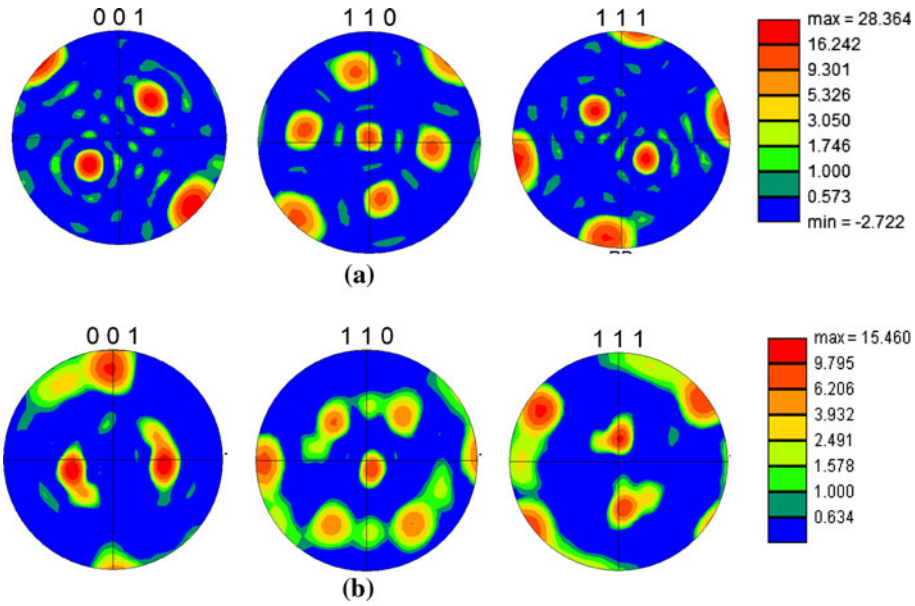

Fig. 5 Pole figures for the sample as-ECAP processed to one pass on plane XY; the shear flow plane (**a**) and the sample ECAP processed to one pass and plane strain compressed to an axial true strain of 1.0 on RD–ND plane (**b**). Please refer to Fig. 1 for checking the planes

represents the evolution of number fraction of high angle grain boundaries (HAGBs), that is, boundaries with misorientation across them greater than 15°. The information for the structure for the samples as-ECAP processed [25] on the *Y–Z* plane is also added for the sake of comparison. Figure 8 represents same information but for the RD–ND plane, the structure information for the samples as-ECAP processed, is as taken on the *X–Y* plane [25], is also included. In the following discussion, the structures of the ECAP and PSC processed samples will be compared to the ones ECAP processed only.

On the RD–TD plane, compared to E1 samples E105 and E11 exhibited a marked decrease in the cell size, reasonable increase in the average misorientation angle, marked increase in the fraction of cells less than 1 μm, but still the low angle boundaries constituted a major part of the microstructure, around 70% of the scan in E105 and 60% of the scan in E11 were still low angle grain boundaries (LAGBs); thus the structure is dominated with cells and subgrain structure. No sign for dynamic recovery is exhibited. For the sample ECAP processed to four passes (E4), the cell size is 1.16 μm, the cell size did not change after a strain of 0.5 in PSC (E405) and slightly increased to 2.4 μm with further straining in PSC (E41), the misorientation slightly decreased for samples E405 and E41 compared to E4, the fraction of submicron grains increased in E405 and then decreased in E41, the fraction of HAGBs in E405 is almost the same as in E4, then slightly reduced in E41. This slight decrease in local misorientation and fraction of HAGBs and slight increase in cell size for E41 can be an indication of dynamic recovery due to the re-arrangements of dislocations into new sub-boundaries with low angle of misorientation. For the sample ECAP processed to eight passes (E8) the cell size is 0.88 μm, the cell size for sample E805 is reduced to 0.5 μm and then increased to 1 μm in E81, the misorientation angle is reduced for both samples, the fraction of submicron grains is greatly enhanced to 96% for E805, and then reduced one more time in E81, the fraction of HAGBs is slightly reduced for both samples. The results also indicate presence of dynamic recovery for both samples; E805 and E81. For the sample ECAP processed to 12 passes (E12) the cell size is 0.6 μm, the cell size in E1205 almost did not change and then got reduced to 0.4 μm for E121, the misorientation angle was slightly higher for E1205 and E121 samples, the fraction of submicron grains in E1205 remained the same as E12, around 90%, as for E121 the fraction was almost 100%, the fraction of HAGBs in E1205 and E121 was found to be slightly higher than E12. The slightly higher local misorientations, the slightly higher fraction of HAGBs and the slight reduction in cell size are all indications that dynamic recovery was suppressed for samples E1205 and E121 and probably dynamic recovery has happened at an earlier stage during the ECAP deformation, specially that the misorientation angle for E12 is slightly lower than E8. For the sample ECAP processed to 16 passes (E16), the cell size is 0.64 μm which is slightly increased in E1605 to 0.99 μm and then again slightly reduced to 0.68 μm in E161, the misorientation angle is reduced markedly for both samples (E1605 and E161), the fraction of submicron grains and HAGBs are also reduced for both samples compared to E16. This strongly suggests the occurrence of considerable dynamic recovery or recrystallization in the post ECAP deformed samples.

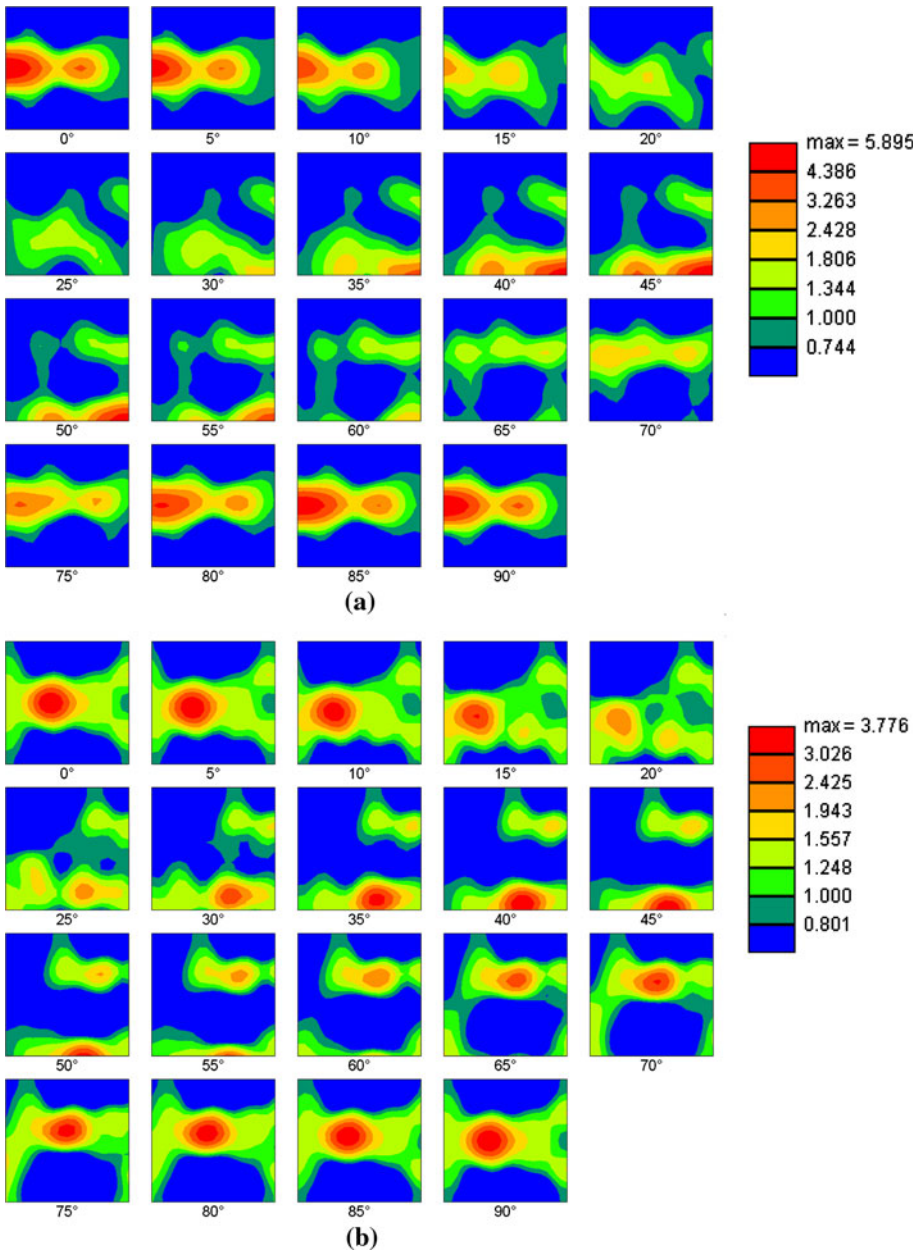

Fig. 6 ODF plots for samples E1205 (**a**), E121 (**b**), E1605 (**c**), and E161 (**d**)

On the RD–ND plane the cell size was found to be almost consistently higher for all tested conditions compared to the RD–TD plane, except for sample E1605.

There was no much change in the cell size with post ECAP deformation on that plane except for the samples that were ECAP processed to one and four passes. On the RD–ND plane the samples that were ECAP processed to 8, 12, and 16 passes and further plane strain compressed exhibited average misorientation angles that were markedly higher than their counterpart on the RD–TD plane, as well as higher than for the samples that were ECAP processed only. The samples ECAP processed to one and four passes and further plane strain compressed exhibited smaller misorientation angle on the RD–ND plane compared to the RD–TD plane, but still higher than misorientation angle exhibited by the samples that were ECAP processed only. On the RD–ND plane, there was not much improvement on the fraction of submicron grains in the samples subjected to post ECAP PSC compared to the ones ECAP processed only, except for E1605. This fraction on the RD–ND plane was consistently lower than their counterpart for the RD–TD plane, again except for E1605. The fraction of HAGBs is consistently higher for the samples subjected to ECAP and PSC than those ECAP

Fig. 6 continued

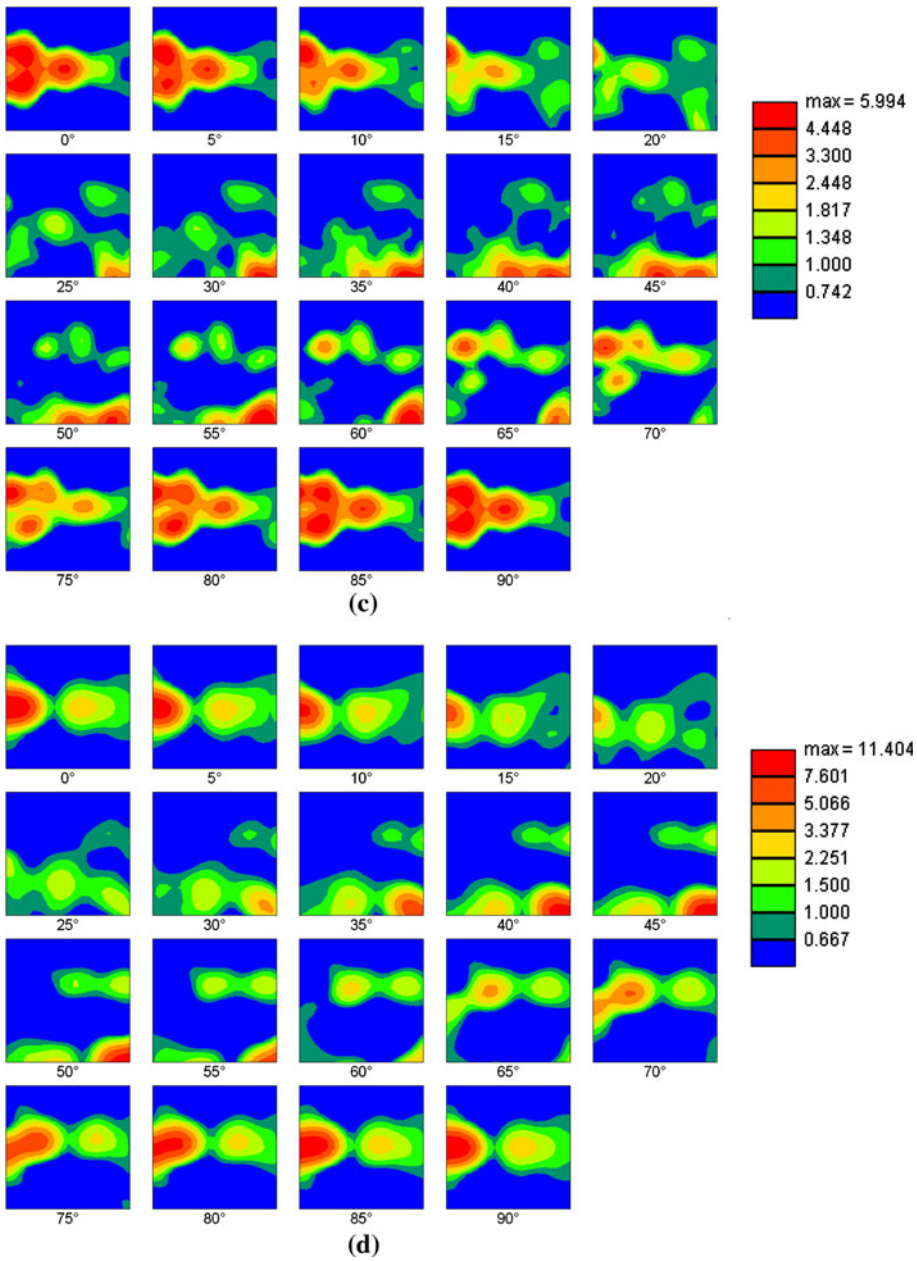

processed only. The value of this fraction is also higher on the RD–ND plane for the samples subjected to 8, 12, and 16 ECAP passes and plane strain compressed than in the RD–TD plane. The fact that the misorientation angle as well as the fraction of HAGBs on the RD–ND plane increased with post ECAP deformation for all loading conditions, may rule out the possibility of dynamic recovery to be happening on that plane, or at least to be predicted by our limited size EBSD scans. The tendency for the average boundary misorientation to change with numbers of ECAP passes as well as with changing the amount of post ECAP deformation in PSC provides a unique opportunity to make use of ECAP and post ECAP processing for the production of materials having controlled boundary misorientation distributions. This suggests the ability to produce UFG materials with different grain boundaries, and this can have a drastic effect on the mechanical behavior of the processed materials.

On the RD–TD plane a decrease in the degree of local misorientation can be noticed in some cases. For example sample E1605 compared to E161 in which there is a decrease in the value of the average misorientation as well as in the fraction of HAGBs. This finding is confirmed with less extent, when samples E1205 and E121 are compared to

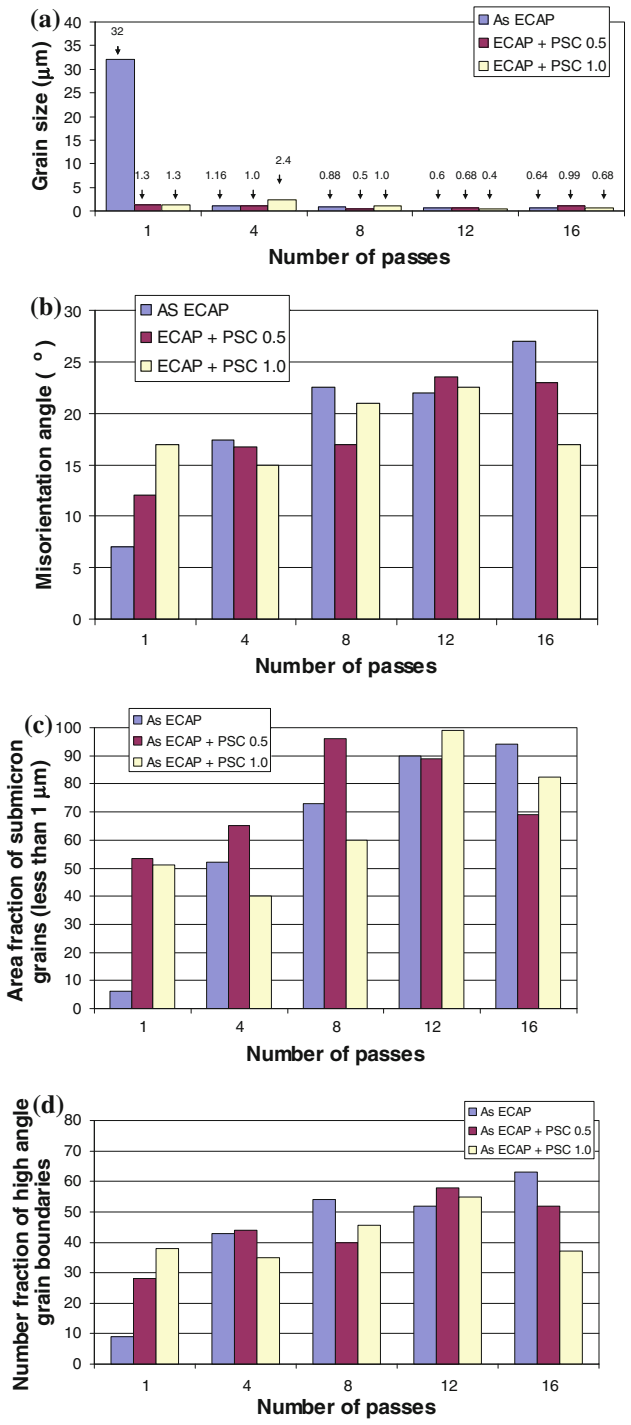

Fig. 7 Variation of grain size based on 2° grain tolerance angle, misorientation angle in the range of 2° to 65°, area fraction of submicron grains and of number fraction of high angle grain boundaries (boundaries with misorientation across them larger than 15°) on the RD–TD plane for samples ECAP processed to different number of passes and samples ECAP processed and further plane strain compressed to axial true strains of 0.5 and 1.0

E1605 and E161, respectively. This decrease in the degree of local misorientation, infers the occurrence of dynamic recovery or recrystallization, which is clearly supported by the observed microstructural features on this plane.

Evolution of ideal rolling texture components

Crystal orientation maps are generated for all samples for the scans performed on the RD–TD plane, in which the main ideal rolling crystallographic orientations exhibited in Table 1, are depicted with a deviation of 10°. These maps have the advantage of revealing the spatial distribution of grains that constitute the main ideal orientations, grains having either these exact orientations or close ones, according to the specified spread angle, are tinted with different colors and a table is provided that correlates the colors to the different orientations. For the sake of saving space and to avoid redundancy, only an example of these maps is presented here. Figure 9 represents a crystal orientation map for sample E81. The key besides the map provides the specific orientations, which are given in Bunge's Euler notation, and the area fraction of each orientation with a 10° spread, which means that all orientations in the data set that lies within the specified spread angle (10° bins in all three Euler angles) from the selected ideal orientations are considered in calculating the fraction values. Figure 10a and b presents the fraction of main rolling orientations as a function of the prior number of ECAP passes and amount of strain in PSC for a spread angle of 10° around the ideal rolling orientations specified in Table 1.

In general, the fraction of the brass component in all samples that were ECAP processed to 4, 8, and 12 passes and further plane strain compressed to an axial true strain of 1.0 was considerably higher than the copper component for the same samples, and also much higher than the brass component in the samples that were plane strain compressed to an axial strain of 0.5. On the contrary to this high brass component phenomenon, samples E105 and E11, displayed a strong copper component and no brass component. The copper component is slightly higher than the brass component for sample E161. It is the other way around for sample E1605, where the brass component is the higher one. An obvious general remark, in the samples that were plane strain compressed to an axial strain of 1.0, is the decrease in the fraction of brass component with the amount of deformation imposed on the sample as a pre-state (number of ECAP passes) to PSC, which could be correlated with the increase in the degree of dynamic

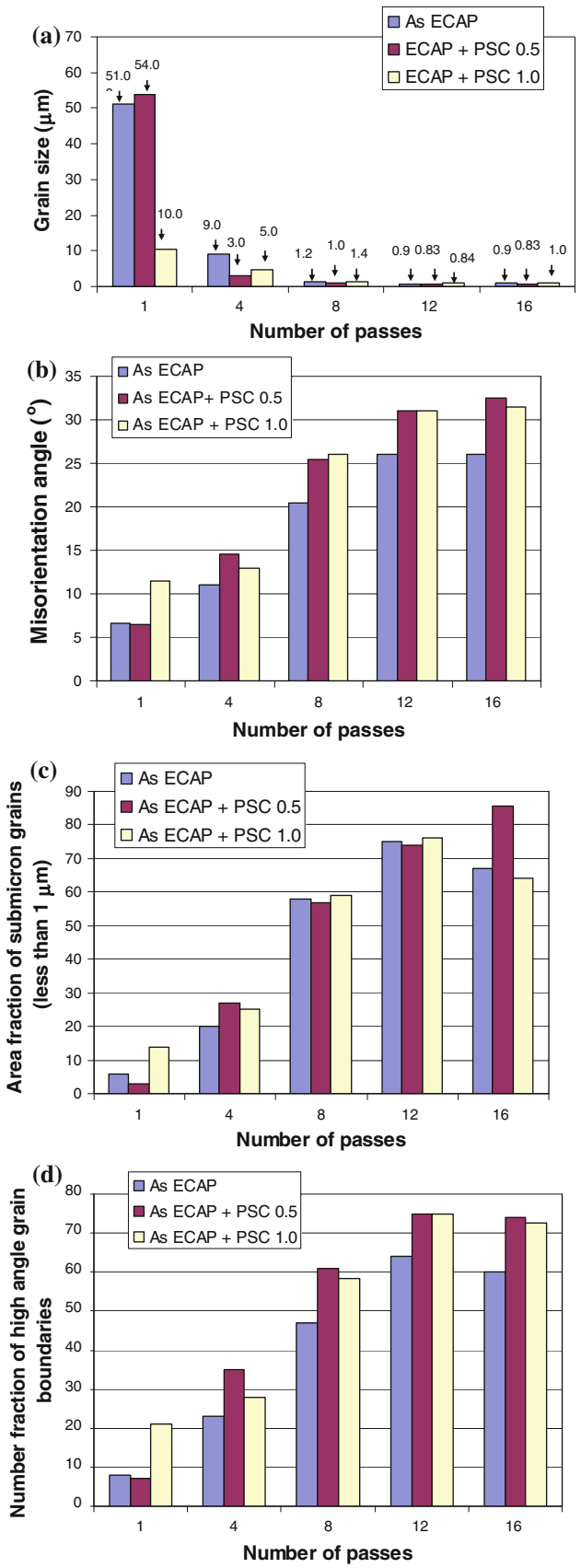

◀ **Fig. 8** Variation of grain size based on 2° grain tolerance angle, misorientation angle in the range of 2° to 65°, area fraction of submicron grains and of number fraction of high angle grain boundaries (boundaries with misorientation across them larger than 15°) on the RD–ND plane for samples ECAP processed to different number of passes and samples ECAP processed and further plane strain compressed to axial true strains of 0.5 and 1.0

recovery and recrystallization observed from the microstructure parameters. The high brass component for some of the aforementioned cases, is an interesting outcome, since it has been always reported [18, 19, 26] that rolling of medium and high stacking fault energy metals, as in the case of the present investigated material, yields copper type texture, but for low stacking fault energy metals the texture is characterized with brass type texture.

Hirsch et al. [18] demonstrated that the copper to brass transition of the rolling texture that happens at intermediate rolling reductions, is mainly related to lowering the stacking fault energy (SFE), and is characterized by an abrupt decrease of the copper component $\{1\ 1\ 2\}\langle 1\ 1\ \bar{1}\rangle$ accompanied by an increase in the orientation density of the copper-twin orientation TC $\{2\ 5\ 5\}\ \langle 5\ 1\ 1\rangle$, due to twinning that with subsequent deformation (rolling), the TC orientation rotates to an intermediate orientation Y $\{1\ 1\ 1\}\ \langle 1\ 1\ 2\rangle$ which

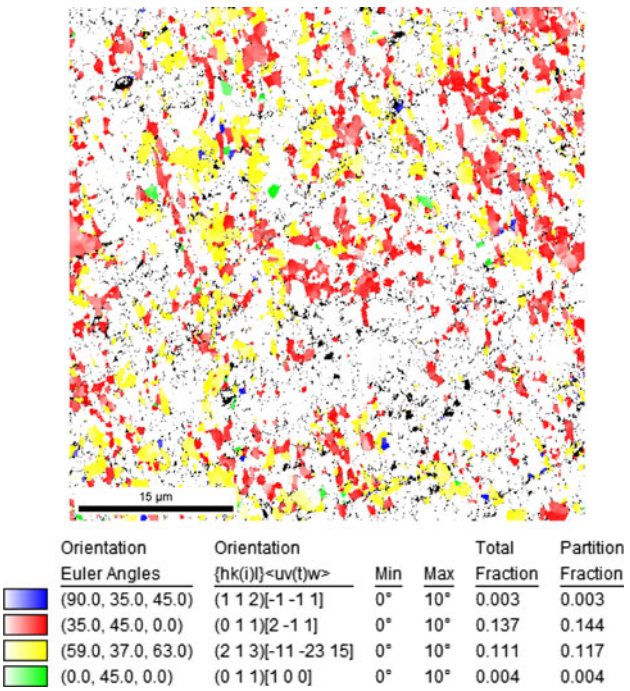

Fig. 9 Crystal orientation maps for sample E81 depicting grains that are with in 10° deviation from the specified ideal rolling orientations listed in the table below and tinted with *different colors* according to the color code in the table

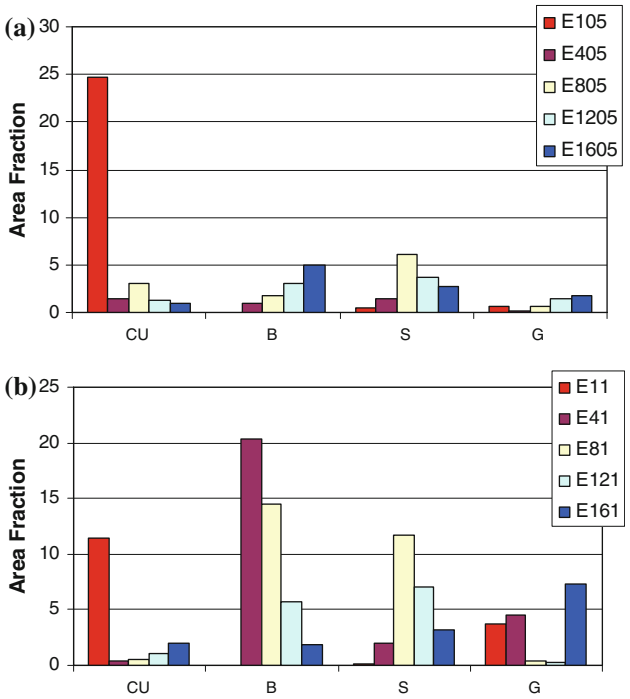

Fig. 10 Fraction of the ideal rolling crystallographic orientations namely copper, brass, S, and Goss orientations with a deviation of 10° for samples ECAP processed to different number of passes and further plane strain compressed to axial true strains of 0.5 (**a**) and 1.0 (**b**)

then rotates to the Goss orientation $\{1\ 1\ 0\}\ \langle 0\ 0\ 1\rangle$, by the process of shear bands. Those authors hypothesized that the Goss orientation is a meta-stable orientation that finally rotates to the stable Brass orientation. This hypothesis is based on the volume fraction of deformation twinning which in our case would be very difficult to form due to the high stacking fault energy of aluminum and ease of cross slipping. Thus, creating such a high brass component and almost negligible copper component, under some loading conditions, in the present material which is considered as a high SFE material is worthy of further investigation and exploitation.

Another hypothesis is that the copper–brass texture transition could be more related to the phenomenon of shear band localization that usually happens in rolling operations [13–15, 27]. In the current work the material before PSC is characterized with considerable stored energy due to the prior deformation from ECAP preloads and highly anisotropic, also the grain structure is considerably small due to the severe plastic deformation involved in the ECAP process. All these aspects can promote shear band localization during PSC. Thus, it is believed that shear banding could play a major role in the plane strain deformation and especially at higher strains (samples that were plane strain compressed to a strain of 1.0). This could be the reason for the high brass components observed for some of the conditions discussed above. Besides, it is logical to think that the crystallites in the shear bands which show preference to the Goss orientation [18] can make a contribution to the rolling texture, as it was previously mentioned that it is only a metastable orientation that rotates with further deformation to the stable brass orientation. The correlation of texture transition from copper to brass with shear banding, rather than with deformation twinning, has been previously asserted [27] for Cu–Zn alloys, with different Zn compositions and consequently different SFE.

Two samples exhibited unique results; sample E105 exhibited a marked high fraction of copper orientation and literally no brass orientation, on the other hand sample E41 exhibited a marked high value for the brass orientation and almost negligible copper orientation. This sample, E41, is a proof that deformation path change could be a very effective tool in manipulating texture, since building such an extremely high brass component and negligible copper component in a high SFE material has not been reported earlier, to the best knowledge of the authors. The higher brass component for some cases (E41, E81, E121, E1205, E1605) can be attributed to shear banding, but the marked increase of this component for sample E41, and the marked increase in the copper component for sample E105 had to be for some other physical reason that could be related to the prior texture to PSC for the RD–TD plane (plane *Y*–*Z* in the as-ECAP processed samples).

A hypothesis that might give an explanation to the high copper orientation in E105 is that the copper orientation might has already been high on the *Y*–*Z* plane of the ECAP processed billet to one pass (E1), as plane strain could be prevailing on that plane, and then got further promoted by the PSC. The same idea holds for sample E41 that exhibited the highest brass orientation, is that sample E4 could already be characterized with a high brass component on the *Y*–*Z* plane of the ECAP processed billet. For that reason, the texture on the *Y*–*Z* plane (which is the same as the RD–TD plane examined after PSC) for the samples that were ECAP processed to one pass (E1) and four passes (E4) was examined and crystal orientation maps were generated. The spread angle was purposely varied from 10° to 15° to 20° around the specified ideal copper and brass orientations. Two scans were made for sample E1, a small scan (75 × 75 μm) with a step size of 0.1 μm and a bigger one (500 × 500 μm) with a step size of 0.5 μm, to get good statistical representative texture data, as the grain size is still relatively large for this sample. Figure 11 shows the crystal orientation maps for these two scans performed for sample E1 for different spread angles. It is obvious the superiority of the copper orientation fraction in this sample. Figure 12 shows the crystal orientation maps for sample E4 for different spread angles. Again, the superiority of the

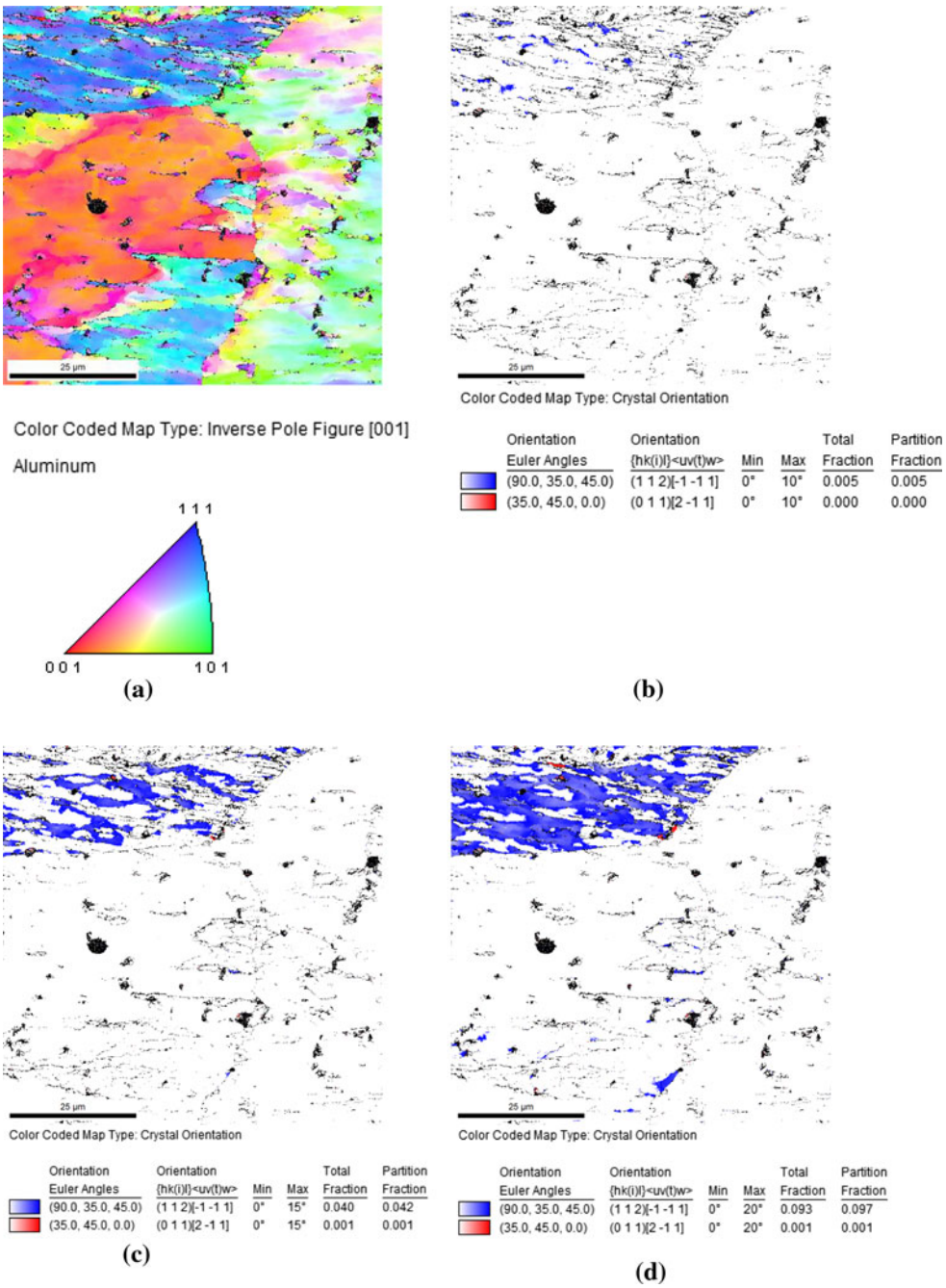

Fig. 11 Crystal orientation maps for sample E1 on the *Y–Z* plane for different spread angles around the ideal copper orientation and ideal brass orientation. The spread angle and the respective color of each orientation are stated in the table underneath the respective maps. **a–d** are taken for a scan 75 × 75 μm with a step size of 0.1 μm. **e–h** are taken for a scan on the same sample on the same plane 500 × 500 μm with a step size of 0.5 μm

brass orientation fraction is obvious. Figure 13 shows the crystal orientation maps for samples E105 in (a–c) and samples E41 in (d–f) for different spread angles. The maps presented in Figs. 11, 12, and 13 depicted only the spread around the copper and brass orientations. Figure 14a and b presents the fraction of copper orientation for samples E1 and E105 and fraction of the brass orientation for samples E4 and E41, respectively. It is obvious that the high fraction of copper orientation in E105 and high fraction of brass orientation in E41 are related to the prior texture in the samples imposed by the ECAP process. Thus, this result strongly points to the effect of initial texture prior to PSC, and in a way contradicts the findings of Ferrasse et al. [6] where they stated that initial texture play a limited role on texture orientations.

Combining ECAP with subsequent upsetting parallel to the extrusion direction has been reported recently [10]. Samples of 1050 AA were ECAP processed via route B_C and route C (180° rotation between subsequent passes) to eight passes and then simple compressed to a true strain of 1.0.

Fig. 11 continued

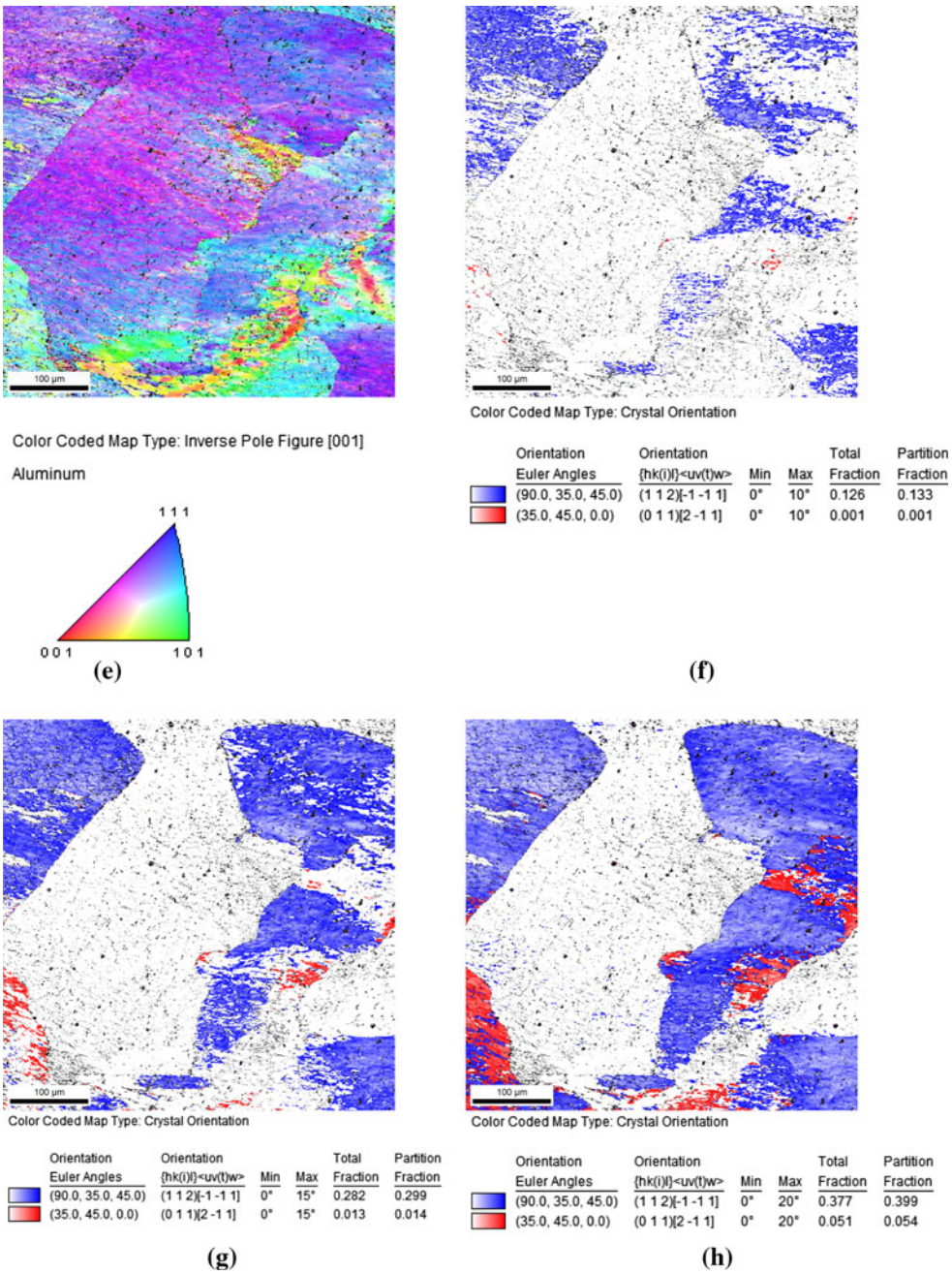

It is reported that the texture transforms from the ECAP texture to the uniaxial compression texture where we have a buildup of a strong [110] fiber texture component, and a decrease in the [100] and [111] fiber texture components, similar to the texture observed in compression of medium and high stacking fault energy materials [27]. Similar texture transition was seen previously with low stacking fault energy (SFE) alloy MP35N [27]. MP35N was simple sheared, using a double shear specimen, to a shear strain of 1.0 and the sheared gage section was wire cut to cubic specimen that was compressed to a true strain of 0.4. Again a clear transition of texture was observed.

Conclusions

Combining ECAP with subsequent deformation, in this case PSC which simulates the rolling operation, can be an effective technique to control texture as well as in producing UFG materials.

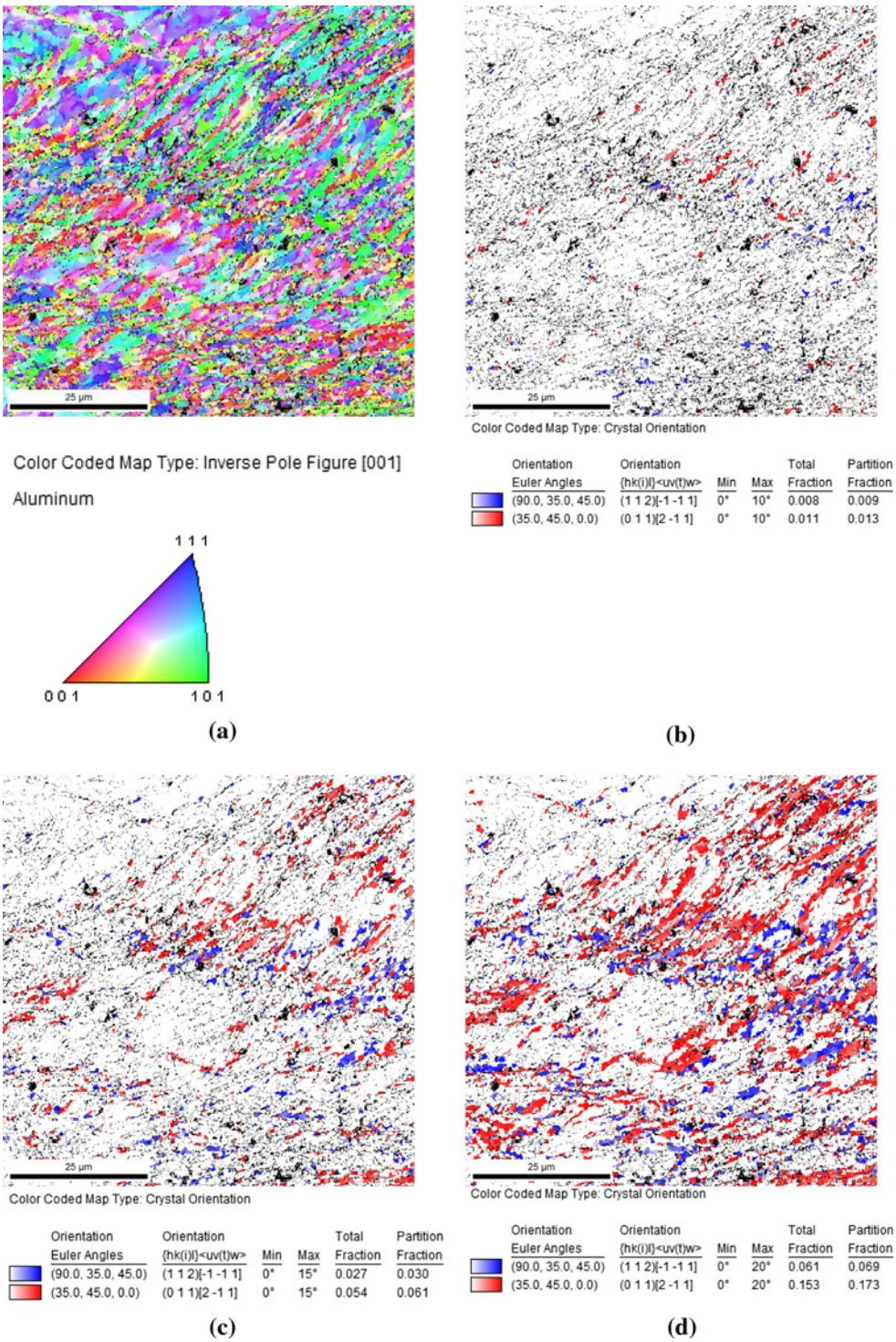

Fig. 12 Crystal orientation maps for sample E4 on the *Y–Z* plane for different spread angle around the ideal copper orientation and ideal brass orientation. The spread angle and the respective color of each orientation are stated in the table underneath the maps

Texture transition from ECAP texture to rolling texture is evident when ECAP was combined with subsequent PSC.

The sample ECAP processed to one pass and plane strain compressed to an axial strain of 0.5 exhibited a marked increase in the fraction of copper orientation and the sample ECAP processed to four passes and further plane strain compressed to an axial strain of 1.0 exhibited a marked increase in the fraction of brass orientation. This was found to be related to the initial texture acquired by the ECAP process.

The extensive plastic strain associated with ECAP and further straining in PSC is thought to be capable of

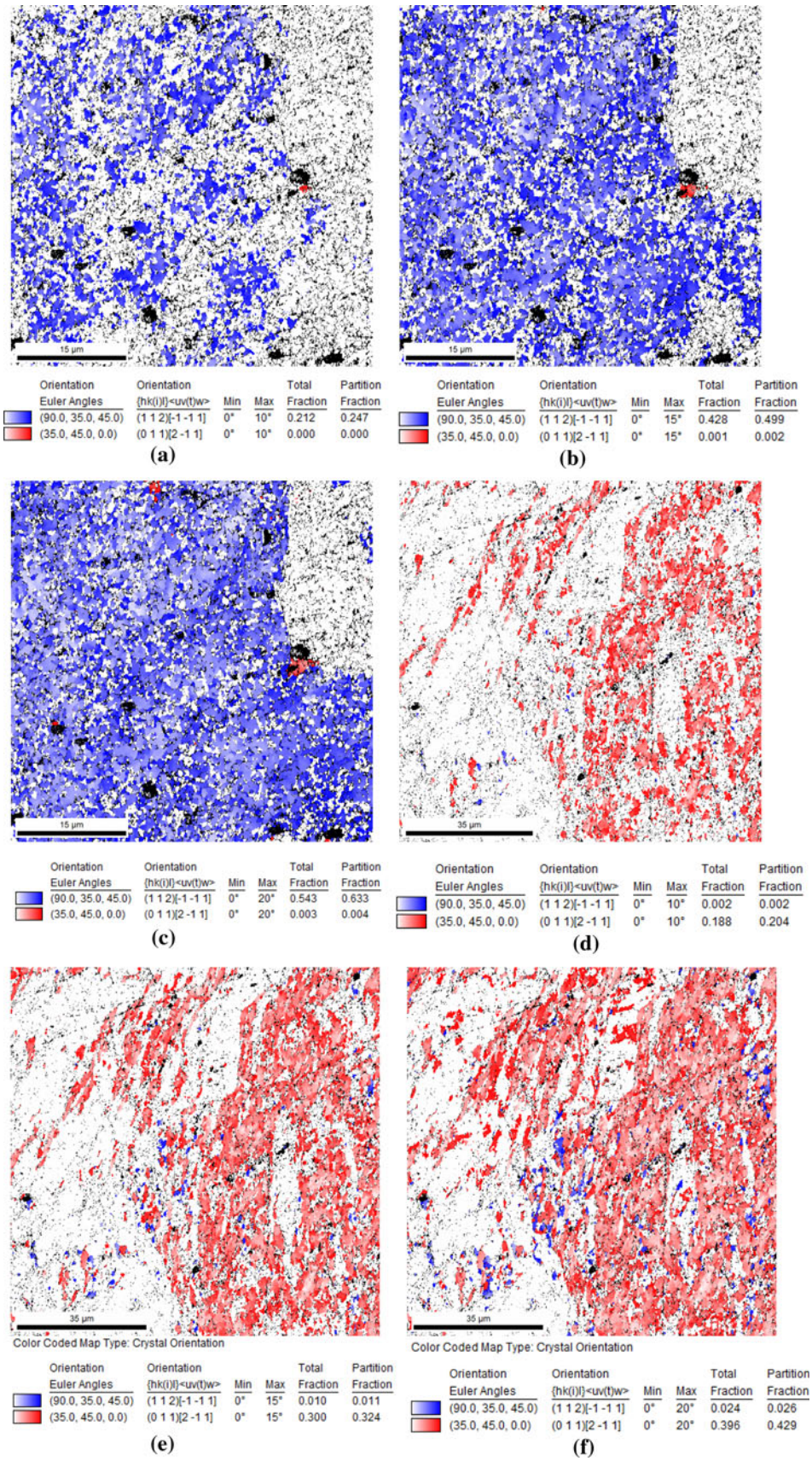

Fig. 13 Crystal orientation maps for samples E105 (**a**–**c**) and E41 in (**d**–**f**) for different spread angle around the ideal copper orientation and ideal brass orientation. The spread angle and the respective color of each orientation are stated in the table underneath the respective maps

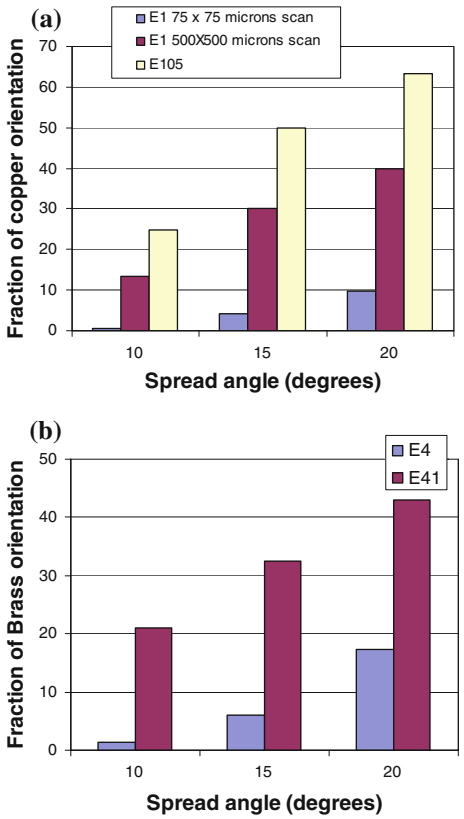

Fig. 14 Fraction of the copper orientation in samples E1 for two different scan sizes (75 × 75 and 500 × 500 μm) and sample E105 (**a**). Fraction of the brass orientation in samples E4 and E41 (**b**). Both sections shows the fraction for different spread angles of 10°, 15°, and 20°

producing a global decrease in texture strength by promoting mechanically induced dynamic recovery which is asserted by the decrease in local misorientation in some of the tested conditions.

Acknowledgement The authors would like to express their sincere thanks for the Center of Excellence for Research in Engineering Materials (CEREM) for the support of this work.

References

1. Aida T, Matsuki K, Horita Z, Langdon TG (2001) Scripta Mater 44:575
2. Iwahashi Y, Wang J, Horita Z, Nemoto M, Langdon TG (1996) Scripta Mater 35:143
3. Zhilyaev AP, Lee S, Nurislamova GV, Valiev RZ, Langdon TG (2001) Scripta Mater 44:2753
4. Iwahashi Y, Horita Z, Nemoto M, Langdon TG (1998) Acta Mater 46:3317
5. Sun P, Kao P, Chang C (2004) Metall Trans A 35A:1359
6. Ferrasse S, Segal VM, Kalidindi SR, Alford F (2004) Mater Sci Eng A 368:28
7. Zhilyaev AP, Swisher DL, Oh-ishi K, Langdon TG, McNelley TR (2006) Mater Sci Eng A 429:137
8. Gholinia A, Prangnell PB, Markushev MV (2000) Acta Mater 48:1115
9. Salem AA, Langdon TG, McNelly TR, Kalidindi SR, Semiatin S (2006) Metall Trans A 37:2879
10. El-Danaf (2008) In: Proceedings of the ASME 2nd multifunctional nanocomoposites and nanomaterials conference, pp 199–211
11. Lapovok R, Timokhina I, McKenzie PWJ, O'Donnell R (2008) J Mater Process Technol 200:441
12. Li S, Beyerlein IJ, Alexander DJ, Vogel SC (2005) Scripta Mater 52:1099
13. Duggan BJ, Hatherly M, Hutchinson WB, Warkefield PT (1978) Metal Sci 12:343
14. El-Danaf E (2002) J Eng Appl Sci 49:493
15. Mohamed AAS, El-Danaf EA, Radwan AA (2007) J Mater Process Technol 186:14
16. Leffers T, Sorensen BJ (1990) Acta Mater 38:1917
17. Seveliano JG, Houtte PV, Aernoudt E (1977) Scripta Metall 11:581
18. Hirsch J, Lucke K (1988) Acta Metal 36:2863
19. Leffers T, Ray RK (2009) Prog Mater Sci 54:351
20. Ferrasse S, Segal VM, Alford F (2004) Mater Sci Eng A 372:44
21. Segal VM (2002) Mater Sci Eng A 338:331
22. El-Danaf EA, Soliman, Almajid AA (2010) Mater Sci Eng A 527:2547
23. Mishra A, Kad BK, Gregori F, Meyers MA (2007) Acta Mater 55:13
24. El-Danaf EA (2008) Mater Sci Eng A 492:141
25. El-Danaf EA (2008) Mater Sci Eng A 487:189
26. Wenk HR, Houtte PV (2004) Rep Prog Phys 67:1367
27. El-Danaf EA, Kalidindi SR, Doherty RD, Necker C (2000) Acta Mater 48:2665